Spin-Orbit Mapping of Light

Liang Fang,[†] Hongya Wang,[†] Yize Liang, Han Cao, and Jian Wang[*]
Wuhan National Laboratory for Optoelectronics and School of Optical and Electronic Information, Huazhong University of Science and Technology, Wuhan 430074, Hubei, China

(Received 3 June 2021; accepted 18 October 2021; published 29 November 2021)

Spin-orbit photonics, involving the interaction between the spin angular momentum (SAM) and orbital angular momentum (OAM) of light, plays an important role in modern optics. Here, we present the spin-orbit mapping of light in a few-mode fiber that originates from the mode degeneracy lifting (TM_{01} and TE_{01}) property. We demonstrate two kinds of spin-orbit mapping phenomena, i.e., mapping from intrinsic SAM to OAM and mapping from polarization direction rotation to field pattern rotation. The demonstrated spin-orbit mapping shows high efficiency, large bandwidth, availability for short pulses, and scalability to high-order OAM states.

DOI: 10.1103/PhysRevLett.127.233901

The spin-orbit optical phenomenon is a common electromagnetic effect arising from the interaction between the polarization (spin) and spatial (orbit) degrees of freedom of light [1–3]. Generally, the continuous polarization rotation of light can carry the spin angular momentum (SAM) [4–7], while the helical phase structure or field pattern rotation of light can produce the orbital angular momentum (OAM) [6–9]. The spin-orbit interaction of light generally originates from the fundamental properties of Maxwell's equations. Two important fundamental concepts, known as the angular momentum and geometric phase, form the basis of spin-orbital interaction of light [3]. The SAM and OAM, as well as the spin-orbit interaction of light, play crucial roles in modern optics [2,3,10–15]. They have greatly promoted the understanding of the fundamentals of light and also facilitated various emerging applications [2,3,15–17], such as optical manipulation [18–21], optical imaging [22,23], optical metrology [24–27], quantum information processing [28–31], and optical communications [32–37].

The common spin-orbit interaction of light can be generally summarized as spin-dependent splitting in Fig. 1(a) and spin-orbit conversion in Fig. 1(b). The spin-dependent splitting in Fig. 1(a) is ruled by the geometric phase, resulting in the splitting or deflection of the propagation of light. Such a phenomenon can be regarded as the photonic spin-Hall effect [10,15,38,39], which is analogous to the classical Stern-Gerlach effect in a field gradient [40–42]. The medium in Fig. 1(a) typically contains polarization gratings, metasurfaces, fibers, and various optical interfaces, such as air-glass and metal-dielectric interfaces [3,15,38,39,43,44]. The spin-orbit conversion in Fig. 1(b) is usually associated with the geometric phase induced by any inhomogeneous transformation of the optical polarization [1,45]. In this case, an inhomogeneous anisotropic medium, such as *q*-plate and metasurfaces [1,29,45], is usually used for spin-orbit conversion. In the process of such spin-orbit conversion, the incident SAM-carrying light beam is converted to the output light beam carrying both OAM and inversed SAM after passing through the inhomogeneous anisotropic medium, i.e., there still exists SAM in the output light beam [1]. Note that the conventional spin-orbit conversion does not simply follow the angular momentum conservation for the input and output light beams, since the inhomogeneous anisotropic medium also gives an additional angular momentum to the light beams. Recently, all-fiber OAM mode generators are also exploited by means of the pressure-induced birefringence for mode synthesis [46] and the coupling of vector modes [47–50]. For the latter, i.e., the conversion from the input SAM-carrying light beam to the output light beam carrying both OAM and SAM [47–50], it can be also categorized as the case in Fig. 1(b).

Beyond the spin-dependent splitting and spin-orbit conversion, here we present another new spin-orbit optical phenomenon in an isotropic medium, namely, spin-orbit

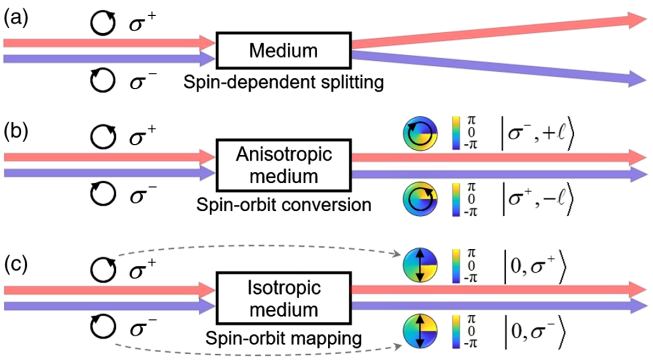

FIG. 1. Spin-orbit optical phenomena. (a) Spin-dependent splitting. (b) Spin-orbit conversion. (c) Spin-orbit mapping.

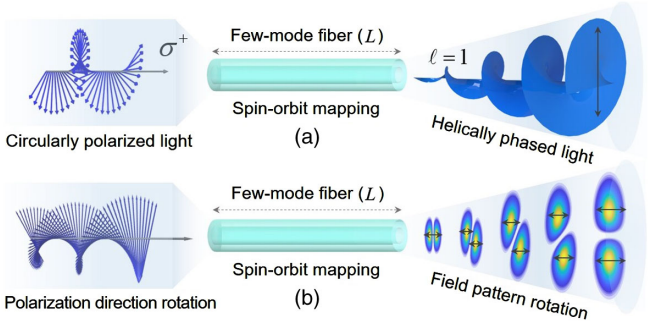

FIG. 2. Spin-orbit mapping using a piece of few-mode fiber. (a) Mapping from intrinsic SAM to OAM. (b) Mapping from polarization direction rotation (SAM) to field pattern rotation (OAM).

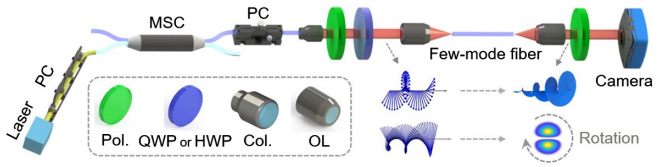

FIG. 3. Experimental configuration for spin-orbit mapping. PC: polarization controller; MSC: mode-selective coupler; Pol.: polarizer; QWP: quarter-wave plate; HWP: half-wave plate; Col.: collimator; OL: objective lens.

mapping. As shown in Fig. 1(c), the spin-orbit mapping means that the SAM carried by the incident light beam is completely converted or transferred to the OAM of the output light beam, i.e., there is no SAM in the output light beam. It should be emphasized that this spin-orbit mapping in an isotropic medium satisfies the angular momentum conservation for the input and output light beams.

In this work, we propose and demonstrate the spin-orbit mapping using a piece of few-mode fiber, which can be regarded as an isotropic medium (homogeneous along azimuthal direction). It can be the conventional few-mode fiber with a center core or the ring-core fiber supporting TM_{01} and TE_{01} eigenmodes with slight effective refractive index difference [51–54]. As illustrated in Fig. 2, there are two kinds of spin-orbit mapping phenomena. One is the mapping from intrinsic SAM to OAM of light beams, as shown in Fig. 2(a); while the other is the mapping from polarization direction rotation to field pattern rotation of light beams, as shown in Fig. 2(b). For the former one, the SAM carried by the incident circularly polarized light beam is fully transferred to the OAM carried by the output helically phased light beam (fixed linear polarization). For the latter one, the polarization direction rotation of the incident light beam (fixed field pattern) is converted to the field pattern rotation of the output light beam (fixed polarization direction). Note that the polarization direction rotation and field pattern rotation in Fig. 2(b) also give SAM and OAM, respectively [6,7,9]. Hence, the latter one with the mapping from polarization direction rotation (SAM) to field pattern rotation (OAM) also belongs to the category of spin-orbit mapping.

We consider a proof-of-concept experimental study on the two kinds of spin-orbit mapping phenomena in Fig. 2. The experimental configuration is shown in Fig. 3 (see more details in the Supplemental Material [55]), where a proper length of weakly guiding few-mode fiber is employed. A home-made all-fiber fused mode-selective coupler (MSC) is adopted to generate the light beam with two lobes [50]. For the mapping from intrinsic SAM to OAM in Fig. 2(a), a quarter-wave plate (QWP) is used to produce the incident circularly polarized light beam carrying SAM. For the mapping from polarization direction rotation to field pattern rotation in Fig. 2(b), a half-wave plate (HWP) is used to control the polarization rotation of the incident light beam.

Before presenting the experimental results, we first describe the underlying mechanisms and give theoretical analyses of spin-orbit mapping phenomena.

We exploit the spatial modes in the first-order mode group of the few-mode fiber, which can be described by either vector eigenmode basis $(\mathrm{TM}_{01}, \mathrm{TE}_{01}, \mathrm{HE}_{21}^{\mathrm{even}}, \mathrm{HE}_{21}^{\mathrm{odd}})$ or angular momentum mode basis $(|\sigma, \ell\rangle = |-1,+1\rangle, |+1,-1\rangle, |+1,+1\rangle, |-1,-1\rangle$ with σ for SAM and ℓ for OAM). It is worth noting that the angular momentum mode basis and vector eigenmode basis can be deduced from each other as $|-1,+1\rangle = \mathrm{TM}_{01} + i\mathrm{TE}_{01}$, $|+1,-1\rangle = \mathrm{TM}_{01} - i\mathrm{TE}_{01}$, $|+1,+1\rangle = \mathrm{HE}_{21}^{\mathrm{even}} + i\mathrm{HE}_{21}^{\mathrm{odd}}$, and $|-1,-1\rangle = \mathrm{HE}_{21}^{\mathrm{even}} - i\mathrm{HE}_{21}^{\mathrm{odd}}$ (see more details in the Supplemental Material [55]).

Generally, the incident light beam synthesized by the linear combination of four angular momentum modes in the first-order mode group can be expressed as $\mathbf{E}_{\mathrm{in}} = \alpha_1|-1,+1\rangle + \alpha_2|+1,-1\rangle + \alpha_3|+1,+1\rangle + \alpha_4|-1,-1\rangle$, which is simply written by

$$\mathbf{E}_{\mathrm{in}} = [\alpha_1, \alpha_2, \alpha_3, \alpha_4]^T, \tag{1}$$

where α_1, α_2, α_3, and α_4 are the coefficients, and the symbol T denotes the transposition. Remarkably, in the first-order mode group, the $\mathrm{HE}_{21}^{\mathrm{even}}$ and $\mathrm{HE}_{21}^{\mathrm{odd}}$ modes are highly degenerated with almost the same mode effective refractive index, while the TM_{01} and TE_{01} modes have slightly different mode effective refractive index (mode degeneracy lifting). Hence, the fiber propagation under the angular momentum mode basis can be described by a transfer matrix

$$\mathbf{M}(z) = \begin{bmatrix} \cos(\delta\beta z) & i\sin(\delta\beta z) & 0 & 0 \\ i\sin(\delta\beta z) & \cos(\delta\beta z) & 0 & 0 \\ 0 & 0 & 1 & 0 \\ 0 & 0 & 0 & 1 \end{bmatrix}, \tag{2}$$

where $\delta\beta = \Delta\beta/2 = (\beta_{TM_{01}} - \beta_{TE_{01}})/2$ with $\beta_{TM_{01}}$ and $\beta_{TE_{01}}$ the propagation constants of TM_{01} and TE_{01} modes, respectively. The output light beam after propagating through the fiber can be written by

$$\mathbf{E}_{out} = \mathbf{M}(z) \cdot \mathbf{E}_{in}. \tag{3}$$

For the spin-orbit mapping from intrinsic SAM to OAM, we employ the incident light beam carrying only SAM expressed as $[0, 1, \pm 1, 0]^T$ (left-handed circularly polarized light beam with $\sigma = +1$ and $\ell = 0$) or $[1, 0, 0, \pm 1]^T$ (right-handed circularly polarized light beam with $\sigma = -1$ and $\ell = 0$). After propagating through a proper fiber length $[L = (2n + 1)\pi/|\Delta\beta|,\ n = 0,\ 1,\ 2,\ldots]$ with the accumulated phase shift between TM_{01} and TE_{01} of $(2n + 1)\pi$, the output light beam becomes $[1, 0, \pm 1, 0]^T$ (linearly polarized OAM-carrying light beam with $\sigma = 0$ and $\ell = +1$) or $[0, 1, 0, \pm 1]^T$ (linearly polarized OAM-carrying light beam with $\sigma = 0$ and $\ell = -1$). Note that the output is still linearly polarized OAM-carrying light beam even considering the relative phase shift between TM_{01}/TE_{01} and $HE_{21}^{even}/HE_{21}^{odd}$. From the input $[0, 1, \pm 1, 0]^T$ ($\sigma = +1$, $\ell = 0$) or $[1, 0, 0, \pm 1]^T$ ($\sigma = -1$, $\ell = 0$) to the output $[1, 0, \pm 1, 0]^T$ ($\sigma = 0$, $\ell = +1$) or $[0, 1, 0, \pm 1]^T$ ($\sigma = 0$, $\ell = -1$), it is easy to understand the spin-orbit mapping phenomenon, where the SAM is, in principle, completely transferred to the OAM. Actually, from the perspective of angular momentum superposition [56–58], we can deduce the mean SAM per photon carried by the propagating light beam along the fiber, approximately expressed as

$$S_{SAM}(z) \approx \frac{1}{2}\sigma[1 + \cos(\Delta\beta z)]\hbar, \tag{4}$$

and the mean OAM per photon

$$L_{OAM}(z) \approx \frac{1}{2}[\ell - \sigma\cos(\Delta\beta z)]\hbar, \tag{5}$$

where $\sigma = +1$, $\ell = +1$ or $\sigma = -1$, $\ell = -1$ and $\hbar$ is the reduced Plank constant. The total angular momentum per photon can be given by $S_{SAM}(z) + L_{OAM}(z) \approx (\ell + \sigma) \cdot \hbar/2 = J$, which is propagation independent. It proves that the total angular momentum is conserved during light propagation along the fiber (see more details in the Supplemental Material [55]).

For the spin-orbit mapping from polarization direction rotation to field pattern rotation, we employ the linearly polarized incident light beam expressed as $[1, 1, 1, 1]^T$ (similar principles for other linearly polarized incident light beams: $[1, -1, 1, -1]^T$, $[1, -1, -1, 1]^T$, $[1, 1, -1, -1]^T$). The incident light beam with linear polarization rotation (by rotating the HWP in Fig. 3) can be expressed as $[e^{i2\theta}, e^{-i2\theta}, e^{-i2\theta}, e^{i2\theta}]^T$, where $\theta = \Omega t$ is the rotating angle of the HWP and Ω is the angular velocity of the rotating HWP. After fiber propagation with a proper length of $L = (2n + 1)\pi/|\Delta\beta|$ ($n = 0,\ 1,\ 2,\ldots$), the incident polarization direction rotation (fixed field pattern) is mapped to the output field pattern rotation (fixed polarization direction) [59]. In fact, both the polarization direction rotation and field pattern rotation can produce SAM and OAM [6,7,9]. For the incident light beam with linear polarization rotation and fixed field pattern, the mean SAM and OAM per photon can be approximately quantified as $S_{SAM} \approx -2\Omega \cdot \hbar/\omega$ and $L_{OAM} = 0$, respectively, where ω denotes the frequency of light. For the output light beam with field pattern rotation and fixed linear polarization, the mean SAM and OAM per photon can be approximately quantified as $S_{SAM} = 0$ and $L_{OAM} \approx -2\Omega \cdot \hbar/\omega$, respectively [55]. It indicates that, for the spin-orbit mapping from incident polarization direction rotation to output field pattern rotation, the SAM is also, in principle, completely transferred to the OAM.

On the basis of theoretical analyses, we experimentally verify the proposed two kinds of spin-orbit mapping phenomena. The few-mode fiber employed in the experiment is a conventional step-index fiber with the core and cladding radii of 7.4 and 62.5 μm, respectively. It supports six modes including two fundamental ones in the zero-order mode group and four high-order ones in the first-order mode group. The optimal fiber length in the experiment, considering the possible deviation of practically fabricated fiber, is about $L = 0.31$ m.

We then demonstrate the spin-orbit mapping from intrinsic SAM to OAM. We use the optical elements (Laser, MSC, PC, QWP) in Fig. 3 to generate four kinds of incident light beams at 1550 nm carrying only SAM, i.e., $[0, 1, 1, 0]^T$, $[0, 1, -1, 0]^T$, $[1, 0, 0, 1]^T$, and $[1, 0, 0, -1]^T$. The measured results (intensity profiles, interferograms by the tilt interference with a reference Gaussian beam, retrieved phase distributions) for the corresponding output light beams are shown in Figs. 4(a)–4(c), 4(d)–4(f), 4(g)–4(i), and 4(j)–4(l), respectively. From the obtained doughnut-shaped intensity profiles with measured linear polarization, forklike interferograms, and helical phase structures, we can confirm that the incident SAM-carrying light beams are successfully converted to the output OAM-carrying light beams. We measure the efficiency of the spin-orbit mapping by characterizing the weight coefficient (x-/y-polarized $\ell = \pm 1$) of the output light beam. Note that the propagation loss of the very short piece (~0.31 m) of few-mode fiber is negligible. Hence, the measured weight coefficient of the output linearly polarized OAM-carrying light beam can be also regarded as the mapping efficiency. From the practically measured mapping efficiencies in Figs. 4(m)–4(p), i.e., above 90% for all four kinds of incident light beams (minimum, 90.50%; maximum, 96.76%), we can conclude that the intrinsic SAM of the incident light beam is nearly

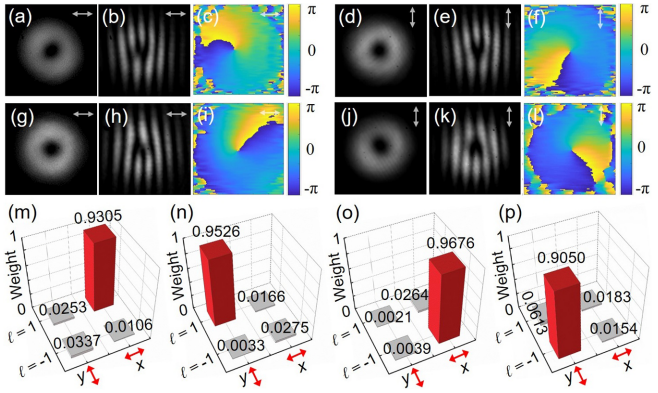

FIG. 4. Measured results for the spin-orbit mapping from intrinsic SAM to OAM. (a)–(c),(m) Mapped output x-polarized $\ell = +1$. (d)–(f),(n) Mapped output y-polarized $\ell = +1$. (g)–(i),(o) Mapped output x-polarized $\ell = -1$. (j)–(l),(p) Mapped output y-polarized $\ell = -1$. (a),(d),(g),(j) Doughnut-shaped intensity profiles. (b),(e),(h),(k) Forklike interferograms. (c),(f),(i),(l) Retrieved helical phase structures. (m)–(p) Measured weight coefficients (mapping efficiencies).

completely mapped to the OAM of the output light beam, which is in good agreement with the theory [55].

We also demonstrate the spin-orbit mapping from polarization direction rotation (SAM) to field pattern rotation (OAM). We use the optical elements (Laser, MSC, PC, HWP) in Fig. 3 to generate the linearly polarized incident light beam, i.e., $[1, 1, 1, 1]^T$. As shown in Fig. 5(a), when rotating the HWP (linear polarization rotation with fixed field pattern of the incident light beam), the field pattern of the output light beam (fixed x polarization) rotates accordingly. Note that there is negligible y-polarization component of the output light beam, which indicates high mapping efficiency. We characterize the linear relationship between the output field pattern rotation and the input linear polarization rotation, as shown in Fig. 5(b). The measured results in Fig. 5 agree well with the theory, indicating the successful

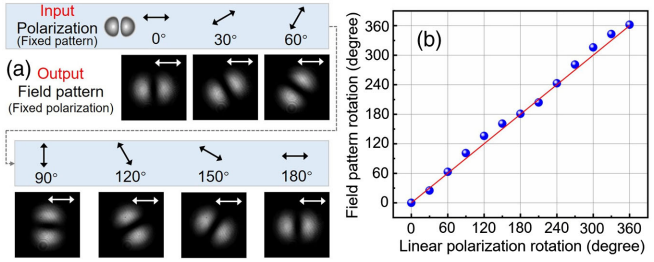

FIG. 5. Measured results for the spin-orbit mapping from polarization direction rotation to field pattern rotation. (a) Measured output field pattern (fixed linear polarization) rotates accordingly when rotating the input linear polarization (fixed field pattern). (b) Measured linear relationship (output field pattern rotation vs input linear polarization rotation). Blue dots: experiment. Red line: theory.

implementation of the spin-orbit mapping from polarization direction rotation (SAM) to field pattern rotation (OAM). Similar results are also obtained for other linearly polarized incident light beams [55].

We further measure the working bandwidth and demonstrate the availability for short pulses of the proposed spin-orbit mapping phenomena. Taking the mapping from intrinsic SAM to OAM as an example, the measured results show a large bandwidth. For an efficiency above 80%, the measured bandwidth is larger than 100 nm; while even for a high efficiency above 90%, the measured bandwidth is larger than 50 nm (see more details in the Supplemental Material [55]). The large bandwidth can be attributed to the fact that the mode degeneracy lifting property (mode effective refractive index difference) of TM_{01} and TE_{01} modes has negligible dependence on the wavelength. We also demonstrate the spin-orbit mapping from intrinsic SAM to OAM for nanosecond or even shorter picosecond pulses in the experiment. The measured results show similar operation performance (high efficiency above 90%) compared to the continuous wave situation (see more details in the Supplemental Material [55]). This is easy to understand based on the measured results that the proposed spin-orbit mapping shows a large bandwidth.

The demonstrated spin-orbit mapping phenomena in Figs. 3–5 are for low-order OAM states with $\ell = \pm 1$. Actually, the proposed spin-orbit mapping can be also scalable to higher-order OAM states with $|\ell| > 1$. To achieve this, instead of four eigenmodes in the first-order mode group, one can employ only two mode degeneracy lifted eigenmodes in the first-order mode group (i.e., TM_{01} and TE_{01}) and the other two highly degenerated eigenmodes in the higher-order mode group (i.e., $HE^{even}_{|\ell|+1,1}$ and $HE^{odd}_{|\ell|+1,1}$ or $EH^{even}_{|\ell|-1,1}$ and $EH^{odd}_{|\ell|-1,1}$, $|\ell| > 1$) to synthesize the incident light beam. The theoretical results show that the input SAM can be also completely transferred to the output OAM after passing through a proper length of fiber. This is applicable to higher-order OAM states with $|\ell| > 1$ for both of the two kinds of spin-orbit mapping phenomena, i.e., mapping from intrinsic SAM to OAM and mapping from polarization direction rotation (local polarization rotation) to field pattern rotation (see more details in the Supplemental Material [55]).

Remarkably, the rigorous separation of the total angular momentum into SAM and OAM is gauge dependent. However, when considering the canonical Noether momentum and spin densities in the Coulomb gauge, this problem of gauge dependence can be solved by a postulate that the vector potential is just evaluated in the transverse part. Although the vector potential is subject to gauge transformations, the quantities defined in terms of the transverse part of the vector potential are gauge invariant [12,60,61]. In the demonstrated spin-orbit mapping phenomena in weakly guiding few-mode fiber, the involved spatial modes are paraxial transverse fields. Therefore, we can consider

the SAM and OAM quantified in the spin-orbit mapping phenomena as gauge invariant.

Generally, the angular momentum is a 3D pseudovector with three spatial components [12,62]. For spatial modes in the weakly guiding few-mode fiber under paraxial approximation condition, there are negligible longitudinal components of electromagnetic fields, which give rise to nearly zero transverse SAM and OAM normal to the direction of propagation. Hence, here we only consider the dominant longitudinal SAM and OAM.

In summary, we theoretically and experimentally demonstrate new spin-orbit mapping phenomena (mapping from intrinsic SAM to OAM and mapping from polarization rotation to pattern rotation) in the weakly guiding few-mode fiber (isotropic medium and homogeneous along azimuthal direction), which are different from the conventional spin-orbit conversion in an inhomogeneous anisotropic medium. The underlying mechanism of the spin-orbit mapping relies on the inherent mode degeneracy lifting (TM_{01} and TE_{01}). Meanwhile, it also involves the other two highly degenerated eigenmodes. The obtained results show impressive performance (high efficiency, large bandwidth, availability for short pulses, scalability to high-order OAM states). The spin-orbit mapping may find wide interesting applications. For example, the generated OAM light beams (spin-orbit mapping from intrinsic SAM to OAM) can be used in manipulation, trapping, tweezers, microscopy, imaging, sensing, quantum science, and optical communications [16,17]; the generated pattern-rotating light beams (spin-orbit mapping from polarization rotation to pattern rotation) can be used in metrology to detect a rotating particle and determine its rotation direction based on the Doppler effect [24,27]. With future improvement, on-chip devices, spin-orbit transferring at single-photon level, and large OAM single-photon sources [29,30,45,63] are of great significance for the spin-orbit mapping.

This work was supported by the National Key R&D Program of China (2019YFB2203604), the National Natural Science Foundation of China (NSFC) (62125503, 11774116, 61905081), the Special fund of Chinese Postdoctoral Science Foundation (2020T130221), the Chinese Postdoctoral Science Foundation (2019M662596), the Key R&D Program of Hubei Province of China (2020BAB001), and the Science and Technology Innovation Commission of Shenzhen (JCYJ20200109114018750).

*Corresponding author.
jwang@hust.edu.cn
†These authors contributed equally to this work.

[1] L. Marrucci, C. Manzo, and D. Paparo, Optical Spin-to-Orbital Angular Momentum Conversion in Inhomogeneous Anisotropic Media, Phys. Rev. Lett. **96**, 163905 (2006).
[2] F. Cardano and L. Marrucci, Spin-orbit photonics, Nat. Photonics **9**, 776 (2015).
[3] K. Y. Bliokh, F. J. Rodríguez-Fortuño, F. Nori, and A. V. Zayats, Spin-orbit interactions of light, Nat. Photonics **9**, 796 (2015).
[4] J. H. Poynting, The wave-motion of a revolving shaft, and a suggestion as to the angular momentum in a beam of circularly-polarized light, Proc. R. Soc. A **82**, 560 (1909).
[5] R. A. Beth, Mechanical detection and measurement of the angular momentum of light, Phys. Rev. **50**, 115 (1936).
[6] G. Nienhuis, Polychromatic and rotating beams of light, J. Phys. B **39**, S529 (2006).
[7] S. J. van Enk and G. Nienhuis, Photons in polychromatic rotating modes, Phys. Rev. A **76**, 053825 (2007).
[8] L. Allen, M. W. Beijersbergen, R. J. C. Spreeuw, and J. P. Woerdman, Orbital angular momentum of light and the transformation of Laguerre-Gaussian laser modes, Phys. Rev. A **45**, 8185 (1992).
[9] A. Y. Bekshaev, M. S. Soskin, and M. V. Vasnetsov, Angular momentum of a rotating light beam, Opt. Commun. **249**, 367 (2005).
[10] K. Y. Bliokh and Y. P. Bliokh, Conservation of Angular Momentum, Transverse Shift, and Spin Hall Effect in Reflection and Refraction of an Electromagnetic Wave Packet, Phys. Rev. Lett. **96**, 073903 (2006).
[11] K. Y. Bliokh, A. Niv, V. Kleiner, and E. Hasman, Geometrodynamics of spinning light, Nat. Photonics **2**, 748 (2008).
[12] K. Y. Bliokh and F. Noriac, Transverse and longitudinal angular momenta of light, Phys. Rep. **592**, 1 (2015).
[13] A. Aiello, P. Banzer, M. Neugebauer, and G. Leuchs, From transverse angular momentum to photonic wheels, Nat. Photonics **9**, 789 (2015).
[14] D. L. P. Vitullo, C. C. Leary, P. Gregg, R. A. Smith, D. V. Reddy, S. Ramachandran, and M. G. Raymer, Observation of Interaction of Spin and Intrinsic Orbital Angular Momentum of Light, Phys. Rev. Lett. **118**, 083601 (2017).
[15] X. Ling, X. Zhou, K. Huang, Y. Liu, C. Qiu, H. Luo, and S. Wen, Recent advances in the spin Hall effect of light, Rep. Prog. Phys. **80**, 066401 (2017).
[16] S. Franke-Arnold, L. Allen, and M. J. Padgett, Advances in optical angular momentum, Laser Photonics Rev. **2**, 299 (2008).
[17] A. M. Yao and M. J. Padgett, Optical angular momentum: Origins, behavior, and applications, Adv. Opt. Photonics **3**, 161 (2011).
[18] A. T. O'Neil, I. MacVicar, L. Allen, and M. J. Padgett, Intrinsic and Extrinsic Nature of the Orbital Angular Momentum of a Light Beam, Phys. Rev. Lett. **88**, 053601 (2002).
[19] Y. Zhao, J. S. Edgar, G. D. M. Jeffries, D. McGloin, and D. T. Chiu, Spin-to-Orbital Angular Momentum Conversion in a Strongly Focused Optical Beam, Phys. Rev. Lett. **99**, 073901 (2007).
[20] M. J. Padgett and R. Bowman, Tweezers with a twist, Nat. Photonics **5**, 343 (2011).
[21] H. Li, Y. Cao, L. Zhou, X. Xu, T. Zhu, Y. Shi, C. Qiu, and W. Ding, Optical pulling forces and their applications, Adv. Opt. Photonics **12**, 288 (2020).
[22] G. Araneda, S. Walser, Y. Colombe, D. B. Higginbottom, J. Volz, R. Blatt, and A. Rauschenbeutel, Wavelength-scale

errors in optical localization due to spin-orbit coupling of light, Nat. Phys. **15**, 17 (2019).
[23] X. Fang, H. Ren, and M. Gu, Orbital angular momentum holography for high-security encryption, Nat. Photonics **14**, 102 (2020).
[24] M. P. J. Lavery, F. C. Speirits, S. M. Barnett, and M. J. Padgett, Detection of a spinning object using light's orbital angular momentum, Science **341**, 537 (2013).
[25] L. Fang, M. J. Padgett, and J. Wang, Sharing a common origin between the rotational and linear Doppler effects, Laser Photonics Rev. **11**, 1700183 (2017).
[26] A. P. Greenberg, G. Prabhakar, and S. Ramachandran, High resolution spectral metrology leveraging topologically enhanced optical activity in fibers, Nat. Commun. **11**, 5257 (2020).
[27] L. Fang, Z. Wan, A. Forbes, and J. Wang, Vectorial Doppler metrology, Nat. Commun. **12**, 4186 (2021).
[28] R. Fickler, R. Lapkiewicz, W. N. Plick, M. Krenn, C. Schaeff, S. Ramelow, and A. Zeilinger, Quantum entanglement of high angular momenta, Science **338**, 640 (2012).
[29] T. Stav, A. Faerman, E. Maguid, D. Oren, V. Kleiner, E. Hasman, and M. Segev, Quantum entanglement of the spin and orbital angular momentum of photons using metamaterials, Science **361**, 1101 (2018).
[30] J. Liu, I. Nape, Q. Wang, A. Vallés, J. Wang, and A. Forbes, Multidimensional entanglement transport through single-mode fiber, Sci. Adv. **6**, eaay0837 (2020).
[31] Q. Wang, F. Wang, J. Liu, W. Chen, Z. Han, A. Forbes, and J. Wang, High-Dimensional Quantum Cryptography with Hybrid Orbital-Angular-Momentum States through 25 km of Ring-Core Fiber: A Proof-of-Concept Demonstration, Phys. Rev. Applied **15**, 064034 (2021).
[32] J. Wang, J. Yang, I. M. Fazal, N. Ahmed, Y. Yan, H. Huang, Y. Ren, Y. Yue, S. Dolinar, M. Tur, and A. E. Willner, Terabit Free-Space Data Transmission Employing Angular Momentum Multiplexing, Nat. Photonics **6**, 488 (2012).
[33] N. Bozinovic, Y. Yue, Y. Ren, M. Tur, P. Kristensen, H. Huang, A. E. Willner, and S. Ramachandran, Terabit-scale orbital angular momentum mode division multiplexing in fibers, Science **340**, 1545 (2013).
[34] J. Wang, Data information transfer using complex optical fields: A review and perspective, Chin. Optic. Lett. **15**, 030005 (2017).
[35] J. Wang, Twisted optical communications using orbital angular momentum, Sci. China Phys. Mech. Astron. **62**, 034201 (2019).
[36] P. Gregg, P. Kristensen, A. Rubano, S. Golowich, L. Marrucci, and S. Ramachandran, Enhanced spin orbit interaction of light in highly confining optical fibers for mode division multiplexing, Nat. Commun. **10**, 4707 (2019).
[37] J. Wang, Orbital angular momentum communications based on standard multi-mode fiber (invited paper), APL Photonics **6**, 060804 (2021).
[38] O. Hosten and P. Kwiat, Observation of the Spin Hall effect of light via weak measurements, Science **319**, 787 (2008).
[39] X. Yin, Z. Ye, J. Rho, Y. Wang, and X. Zhang, Photonic spin Hall effect at metasurfaces, Science **339**, 1405 (2013).
[40] T. Sleator, T. Pfau, V. Balykin, O. Carnal, and J. Mlynek, Experimental Demonstration of the Optical Stern-Gerlach Effect, Phys. Rev. Lett. **68**, 1996 (1992).
[41] L. Karpa and M. Weitz, A Stern-Gerlach experiment for slow light, Nat. Phys. **2**, 332 (2006).
[42] A. Karnieli and A. Arie, All-Optical Stern-Gerlach Effect, Phys. Rev. Lett. **120**, 053901 (2018).
[43] Z. Bomzon, G. Biener, V. Kleiner, and E. Hasman, Space-variant Pancharatnam-Berry phase optical elements with computer-generated subwavelength gratings, Opt. Lett. **27**, 1141 (2002).
[44] L. Fang and J. Wang, From Imbert–Fedorov shift to topologically spin-dependent walking off for highly confining fiber-guided twisted light, J. Opt. **23**, 065603 (2021).
[45] R. C. Devlin, A. Ambrosio, N. A. Rubin, J. P. Balthasar Mueller, and F. Capasso, Arbitrary spin-to-orbital angular momentum conversion of light, Science **358**, 896 (2017).
[46] S. Li, Q. Mo, X. Hu, C. Du, and J. Wang, Controllable all-fiber orbital angular momentum mode converter, Opt. Lett. **40**, 4376 (2015).
[47] L. Fang and J. Wang, Flexible generation/conversion/exchange of fiber-guided orbital angular momentum modes using helical gratings, Opt. Lett. **40**, 4010 (2015).
[48] L. Fang and J. Wang, Full-vectorial mode coupling in optical fibers, IEEE J. Quantum Electron. **54**, 6800207 (2018).
[49] S. Pidishety, M. I. M. Abdul Khudus, P. Gregg, S. Ramachandran, B. Srinivasan, and G. Brambilla, OAM beam generation using all-fiber fused couplers, in *Proceedings of the Conference on Lasers and Electro-Optics (CLEO)* (Optical Society of America, San Jose, California, 2016), Paper No. STu1F.2.
[50] W. Zhou, H. Cao, L. Wang, and J. Wang, All-fiber orbital angular momentum (OAM) functional devices for mode-division (de)multiplexing in conventional graded-index multimode fiber, in *Proceedings of the Optical Fiber Communication Conference (OFC)* (Optical Society of America, San Jose, California, 2019), Paper No. Th3D.5.
[51] K. Okamoto, *Fundamentals of Optical Waveguides* (Academic Press, San Diego, CA, USA, 2006).
[52] S. Ramachandran, P. Gregg, P. Kristensen, and S. E. Golowich, On the scalability of ring fiber designs for OAM multiplexing, Opt. Express **23**, 3721 (2015).
[53] S. Chen, S. Li, L. Fang, A. Wang, and J. Wang, OAM mode multiplexing in weakly guiding ring-core fiber with simplified MIMO-DSP, Opt. Express **27**, 38049 (2019).
[54] S. Ramachandran and P. Kristensen, Optical vortices in fiber, Nanophotonics **2**, 455 (2013).
[55] See Supplemental Material at http://link.aps.org/supplemental/10.1103/PhysRevLett.127.233901 for details about the experimental setup, angular momentum mode basis, vector eigenmode basis, derivation of spin-orbit mapping, angular momentum evolution, angular momentum conservation, additional results for high-order OAM states, bandwidth measurement, and nanosecond-picosecond short pulses.
[56] G. Molina-Terriza, J. P. Torres, and L. Torner, Management of the Angular Momentum of Light: Preparation of Photons in Multidimensional Vector States of Angular Momentum, Phys. Rev. Lett. **88**, 013601 (2002).

[57] R. Zambrini and S. M. Barnett, Angular momentum of multimode and polarization patterns, Opt. Express **15**, 15214 (2007).

[58] L. Fang and J. Wang, Optical angular momentum derivation and evolution from vector field superposition, Opt. Express **25**, 23364 (2017).

[59] H. Wang, L. Fang, X. Zhang, Y. Liang, and J. Wang, Demonstration of transferring spin-based Pancharatnam-Berry phase to modal orbital rotation in a few mode fiber, in *Proceedings of the Conference on Lasers and Electro-Optics (CLEO)* (Optical Society of America, San Jose, California, 2021), Paper No. JW1A.180.

[60] S. J. van Enk and G. Nienhuis, Eigenfunction description of laser beams and orbital angular momentum of light, Opt. Commun. **94**, 147 (1992).

[61] S. J. van Enk and G. Nienhuis, Spin and orbital angular momentum of photons, Europhys. Lett. **25**, 497 (1994).

[62] L. Fang and J. Wang, Intrinsic transverse spin angular momentum of fiber eigenmodes, Phys. Rev. A **95**, 053827 (2017).

[63] N. Zhou, S. Zheng, X. Cao, Y. Zhao, S. Gao, Y. Zhu, M. He, X. Cai, and J. Wang, Ultra-compact broadband polarization diversity orbital angular momentum generator with $3.6 \times 3.6\ \mu m^2$ footprint, Sci. Adv. **5**, eaau9593 (2019).